INTERNATIONAL JOURNAL FOR NUMERICAL AND ANALYTICAL METHODS IN GEOMECHANICS
Int. J. Numer. Anal. Meth. Geomech., **23**, 629–646 (1999)

THEORETICAL AND NUMERICAL ANALYSES OF CONVECTIVE INSTABILITY IN POROUS MEDIA WITH UPWARD THROUGHFLOW

CHONGBIN ZHAO*, B. E. HOBBS AND H. B. MÜHLHAUS

CSIRO Division of Exploration and Mining, P.O. Box 437, Nedlands, WA 6009, Australia

SUMMARY

Exact analytical solutions have been obtained for a hydrothermal system consisting of a horizontal porous layer with upward throughflow. The boundary conditions considered are constant temperature, constant pressure at the top, and constant vertical temperature gradient, constant Darcy velocity at the bottom of the layer. After deriving the exact analytical solutions, we examine the stability of the solutions using linear stability theory and the Galerkin method. It has been found that the exact solutions for such a hydrothermal system become unstable when the Rayleigh number of the system is equal to or greater than the corresponding critical Rayleigh number. For small and moderate Peclet numbers ($Pe \leqslant 6$), an increase in upward throughflow destabilizes the convective flow in the horizontal layer. To confirm these findings, the finite element method with the progressive asymptotic approach procedure is used to compute the convective cells in such a hydrothermal system. Copyright © 1999 John Wiley & Sons, Ltd.

Key words: exact analytical solution; convective stability; horizontal layer; porous medium; throughflow; finite element analysis

1. INTRODUCTION

Analytical solutions are very important for scientific and engineering problems.[1] For example, an analytical solution can be used as a powerful means to gain an understanding of the solution scenarios under some extreme conditions for a given problem. In addition, an analytical solution is often a useful or even in some circumstances an unique measure in the assessment and validation of any numerical method. However, most scientific and engineering problems are mathematically described by a set of partial differential equations. This makes it extremely difficult to obtain analytical solutions for such problems. As a result, to the best of the authors' knowledge, an analytical solution for a hydrothermal system consisting of a horizontal porous layer with upward throughflow has not been available. Thus, one of the main purposes of this study is to derive analytical solutions for this problem with boundary conditions of constant temperature, constant pressure at the top of the layer and constant vertical temperature gradient, constant Darcy velocity at the bottom of the layer. The governing partial differential equations of the problem consist of a continuity equation, Darcy's equation and an energy balance equation.

*Correspondence to: C. Zhao, CSIRO Division of Exploration and Mining, P.O. Box 437, Nedlands, WA 6009, Australia

CCC 0363–9061/99/070629–18$17.50

Received 26 September 1997
Revised 22 May 1998

As demonstrated in recent studies,[2–4] convective pore-fluid flow driven by a temperature gradient can play a significant role in mineralization and ore body formation in fluid-saturated porous rock masses. It is necessary to study the stability of the trivial solution for the above-mentioned hydrothermal system because only a non-trivial solution results in temperature gradient driven convective flow in such a system. The resulting convective flow can enhance the mixing of species, and therefore promotes mass transport, chemical reactions and mineralization. In this sense, temperature gradient driven convective flow acts as a very powerful catalyst for mineralization in hydrothermal systems. However, the previous studies[2–4] have only dealt with convective instability problems in porous media without upward throughflow. The main difficulty in dealing with convective instability in porous media *with upward throughflow* is that one has to solve a complete fourth-order ordinary differential equation instead of solving an incomplete fourth-order (with the first-order and the third-order terms exactly being zero) ordinary differential equation as in the no upward throughflow case. This will lead to a formidable difficulty in mathematics and therefore, requires to develop a new solution methodology. It is both the consideration of upward throughflow and the newly proposed solution method that make this study significantly different from the previous ones.[2–4]

If no vertical flow goes initially through the layer, the trivial steady-state solutions for temperature and pore-fluid flow become unstable when the Rayleigh number of the layer is equal to or greater than the corresponding critical Rayleigh number. However, if vertical pore-fluid flow occurs initially through the layer, driven by imposed fluid pressure gradients or imposed mass fluxes, the trivial solutions may be stabilized for some boundary conditions but destabilized for other boundary conditions,[5–7] compared with the no initial pore-fluid flow situation. In the case of no initial throughflow, the trivial steady-state temperature profile is caused by heat conduction only, and therefore is linear in the layer thickness direction. In the case of initial throughflow, heat is transferred by both conduction and advection in the layer so that the trivial steady-state temperature profile is non-linear across the thickness of the layer. Because of this significant difference, theoretical research on temperature gradient driven pore-fluid convective instability in porous media with throughflow is very limited. As mentioned above, the main difficulty in dealing with this kind of problem is that one must solve a complete fourth-order ordinary differential equation instead of solving an incomplete fourth-order (with the first-order and the third-order terms identically equal to zero) ordinary differential equation as in the no initial throughflow case. This, to a large extent, has led to the lack of understanding of how the upward throughflow interacts with the convective flow in a porous medium. Besides, little, if any, numerical research has been carried out on this kind of problem. Thus, this paper will focus on both theoretical and numerical analyses of temperature gradient driven pore-fluid convective instability in porous media with upward throughflow.

This kind of convective instability problem has a very strong practical background in geophysics and geoenvironmental engineering. For example, a horizontal layer of a fluid-saturated porous medium may undergo constant temperature and overpressure at its top, whereas it may undergo constant vertical temperature gradient and constant injection of mass flux at its bottom. The overpressure can result from the presence of impermeable seals in geophysics, while it can be induced by surface structures or human activities in geoenvironmental engineering. The vertical temperature gradient may be generated by either geothermal sources in geophysics or buried heat-generating waste in geoenvironmental engineering. The mass flux may be generated by dehydration reactions or by compaction of underlying soft layers or reservoirs. From the

geomechanics point of view, the overpressure will lead to consolidation in the underlying soft layers so that the pore-fluid can be squeezed out of the layer. Compared with convective flow driven by the temperature gradient only, the squeezed pore-fluid flow may be strong at the beginning of the soft layer consolidation, but vanishes at the end of the consolidation. In this situation, it is necessary to study temperature gradient driven pore-fluid convective instability in porous media with decreasing upward throughflow. Clearly, the results from such a study are significant from the following two points of view: (1) If a decrease in upward throughflow destabilizes temperature gradient driven convective flow, then the strongest temperature gradient driven flow takes place at the end of the underlying soft layer consolidation. This implies that if there is no temperature gradient driven convective flow at the end of the consolidation, there is definitely no temperature gradient driven convective flow during the consolidation. (2) If a decrease in upward throughflow stabilizes the temperature gradient driven convective flow, then the strongest temperature gradient driven flow occurs during the consolidation. This means that the existence of the temperature gradient driven convective flow at the end of the consolidation can guarantee the existence of the temperature gradient driven convective flow during the consolidation.

In view of the above, we begin with a statement of the problem, which is followed by the derivation and stability analysis of exact analytical solutions in Section 2. The exact analytical (trivial) solutions are then derived, followed by a stability analysis of the exact solutions using conventional linear stability theory and the Galerkin method. In Section 3, the finite element method with the progressive asymptotic approach procedure[2] is used to confirm the convective flow instability predicted by linear stability theory and the Galerkin method. Finally, some conclusions are given in Section 4.

2. THEORETICAL ANALYSIS

2.1. Statement of the problem

The hydrothermal system considered is a horizontal layer of infinite length and thickness, H, with upward throughflow in a fluid-saturated porous medium. As shown in Figure 1, the boundary conditions are constant temperature and constant pressure at the top of the layer, and constant vertical Darcy velocity and constant vertical temperature gradient at the bottom of the

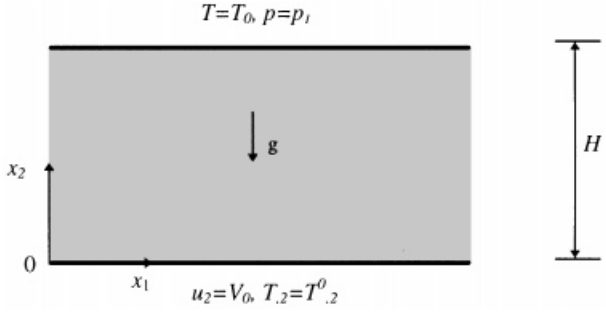

Figure 1. Geometry and boundary conditions of a hydrothermal system

layer. This means that the layer is heated from below. The steady-state governing equations for this hydrothermal system are expressed as [2]

$$u_{i,i} = 0 \tag{1}$$

$$u_i = \frac{1}{\mu} K_{ij}(-p_{,j} + \rho_f g_j) \tag{2}$$

$$(\rho_0 c_p) u_j T_{,j} = (\lambda^e_{ij} T_{,j})_{,i} \tag{3}$$

$$\rho_f = \rho_0[1 - \beta(T - T_0)] \tag{4}$$

$$\lambda^e_{ij} = \phi\lambda_{ij} + (1 - \phi)\lambda^s_{ij} \tag{5}$$

where u_i is the Darcy velocity component in the x_i direction: p and T are pressure and temperature; ρ_0 and T_0 are the reference density of pore-fluid and the reference temperature of the medium; μ and c_p are the dynamic viscosity and specific heat of pore-fluid; λ_{ij} and λ^s_{ij} are the second-order conductivity tensors for the pore-fluid and solid matrix in the porous medium; ϕ and β are the porosity of the medium and the thermal volume expansion coefficient of pore-fluid; K_{ij} is the second-order permeability tensor of the medium and g_i is the gravity acceleration component in the x_i direction.

It is noted that in the fields of geomechanics and geoscience, Darcy's law has been widely used to describe the pore-fluid in fluid-saturated porous media.[8,9] The justification of using Darcy's law can be found in many classical literatures. For example, Nield and Bejan[9] commented that 'Darcy's law has been verified by the results of many experiments. Theoretical backing for it has been obtained in various ways, with the aid of either deterministic or statistical models.' Thus, it is reasonable to use Darcy's law to describe the pore-fluid flow in this study. On the other hand, from the fluid dynamics point of view, Darcy's law, in essence, belongs to the momentum equation, rather than the constitutive equation. In other words, Darcy's law, which is used to describe the pore-fluid flow in a porous medium, is the analog of the Navier–Stokes equation, which is used to describe the fluid flow in a pure fluid medium. Clearly, Darcy's equation (i.e., equation (2)) is coupled with the energy equation (i.e., equation (3)) via both the pore-fluid velocity and the density, which is a function of temperature (see equation (4)). It is the coupling effect between Darcy's equation and the energy equation that plays an important role in the analysis of convective instability in a fluid-saturated porous medium.

The boundary conditions of the problem can be expressed as

$$\begin{aligned} &T = T_0, \quad p = p_1 && (\text{at } x_2 = H) \\ &u_2 = V_0, \quad T_{,2} = T^0_{,2} = -q_0/\lambda_{e0} && (\text{at } x_2 = 0) \end{aligned} \tag{6}$$

where T_0, p_1, V_0, $T^2_{,2}$, λ^0_{e0} and q_0 are constants. Physically, q_0 is the conductive thermal flux and λ_{e0} is a reference conductivity of the porous medium. Thus, q_0 being constant implies that the conductive thermal flux is constant at the bottom of the layer.

Note that if the porous medium of the layer is homogeneous and isotropic, equations (1)–(4) can be written in the following dimensionless form:

$$u^*_{i,i} = 0 \tag{7}$$

$$u^*_i = -p^*_{,i} + \mathrm{Ra}\, T^* e_i \tag{8}$$

$$u^*_j T^*_{,j} = T^*_{,jj} \tag{9}$$

where $\mathbf{e}$ is a unit vector and $\mathbf{e} = e_1\mathbf{i} + e_2\mathbf{j}$ for a two-dimensional problem. Other dimensionless variables are defined as

$$x_i^* = \frac{x_i}{H}, \qquad T^* = \frac{\lambda_{e0}(T - T_0)}{q_0 H}, \qquad u_i^* = \frac{H\rho_0 c_p}{\lambda_{e0}} u_i$$

$$p^* = \frac{K_h \rho_0 c_p}{\mu \lambda_{e0}} (p - p_0), \qquad T_{,2}^* = \frac{\lambda_{e0}}{q_0} T_{,2}$$

$$\mathrm{Ra} = \frac{(\rho_0 c_p)\rho_0 g \beta K_h q_0 H^2}{\mu \lambda_{e0}^2} \tag{10}$$

where x_i^* are the dimensionless coordinates; u_i^* is the dimensionless Darcy velocity component in the x_i direction; p^* and T^* are the dimensionless pressure and temperature; $T_{,2}^*$ is the dimensionless vertical temperature gradient; K_h is a reference medium permeability coefficient in the horizontal direction; Ra is the modified Rayleigh number expressed in terms of the conductive thermal flux rather than in terms of the conventional temperature difference; H is the thickness of the layer and p_0 is the static pore-fluid pressure.

The boundary conditions of the problem in equation (6) can also be written in the dimensionless form as

$$T^* = 0, \qquad p^* = p_1^* \qquad (\text{at } x_2^* = 1) \tag{11}$$

$$u_2^* = Pe = \frac{H\rho_0 c_p}{\lambda_{e0}} V_0, \qquad T_{,2}^* = -1 \qquad (\text{at } x_2^* = 0) \tag{12}$$

where Pe is the Peclet number of the hydrothermal system.

2.2. Derivation of analytical solutions

For the hydrothermal system considered, the trivial solution for the horizontal Darcy pore-fluid velocity is zero.

$$u_1^* = 0 \tag{13}$$

Substituting equation (13) into equation (7) yields the following equation:

$$u_{2,2}^* = 0 \tag{14}$$

It straightforwardly follows from equations (12) and (14) that

$$u_e^* = Pe \tag{15}$$

This indicates that the vertical velocity, which is referred to as upward throughflow in the introduction, is constant throughout the whole layer.

Substituting equations (13) and (15) into equation (9) yields the following equation:

$$Pe\, T_{,2}^2 = T_{,ii}^2. \tag{16}$$

The solution for equation (16) can be expressed as

$$T^* = C_1 \mathrm{e}^{Pe x_2^*} + C_2 \tag{17}$$

where C_1 and C_2 are two independent constants. In order to determine C_1 and C_2 constants uniquely, we have to use two thermal boundary conditions, one of which must be a temperature boundary. Insertion of equations (17) into equations (11) and (12) yields

$$T^* = \frac{1}{Pe}(\mathrm{e}^{Pe} - \mathrm{e}^{Pe x_2^*}). \tag{18}$$

It is noted from equations (8) and (13) that p^* is a function of x_2^* only. Hence,

$$\frac{\partial p^*}{\partial x_2^*} = \frac{\mathrm{d}p^*}{\mathrm{d}x_2^*} = \mathrm{Ra}\, T^* - Pe. \tag{19}$$

Integrating equation (19) with respect to x_2^* yields the following equation:

$$p^* = \frac{\mathrm{Ra}}{Pe}\left(\mathrm{e}^{Pe} x_2^* - \frac{1}{Pe}\mathrm{e}^{Pe x_2^*}\right) - Pe x_2^* + C_3 \tag{20}$$

where C_3 is a constant which can be determined from equation (11):

$$C_3 = p_1^* + Pe - \frac{\mathrm{Ra}}{Pe}\left(\mathrm{e}^{Pe} - \frac{1}{Pe}\mathrm{e}^{Pe}\right). \tag{21}$$

It follows that the final solution for the dimensionless pressure can be expressed as

$$p^* = \frac{\mathrm{Ra}}{Pe}\left(\mathrm{e}^{Pe} x_2^* - \frac{1}{Pe}\mathrm{e}^{Pe x_2^*}\right) - Pe x_2^* + p_1^* + Pe - \frac{\mathrm{Ra}}{Pe}\left(\mathrm{e}^{Pe} - \frac{1}{Pe} e^{Pe}\right) \tag{22}$$

Up to now, we have obtained the exact solutions for the dimensionless Darcy velocities (equations (13) and (15)), dimensionless temperature (equation (18)) and dimensionless pressure (equation (22)) of the hydrothermal system.

2.3. Stability analysis of exact trivial solutions

Next, the stability of the above solution is investigated in a linear stability analysis. Supposing the hydrothermal system is subjected to a small disturbance, the total solutions for the dimensionless velocities, temperature and pressure of the system can be expressed as

$$u_{ti}^* = u_i^* + \hat{u}_i^*, \qquad T_t^* = T^* + \hat{T}^*, \qquad p_t^* = p^* + \hat{p}^* \tag{23a}$$

where $\hat{u}_i^*$, $\hat{T}^*$ and $\hat{p}^*$ are the corresponding perturbation solutions due to the small disturbance. From the linear stability theory point of view, if and only if all these perturbation solutions are zero, then the exact solutions obtained in Section 2.2. are stable. This implies that the stability of the exact solutions for the hydrothermal system considered here can be judged by examining the existence of the non-zero solutions for $\hat{u}_i^*$, $\hat{T}^*$ and $\hat{p}^*$.

Note that the small disturbance may be caused by a small tremor of the earth. From the classical perturbation theory, we can introduce a small parameter, ε, to express the consequence

of this small disturbance. For example, using this small parameter, it is possible to express the resulting perturbation velocity, temperature and pressure of a system in the following form:

$$\hat{u}_i^* = \varepsilon(\hat{u}_i^{*(0)} + \varepsilon\hat{u}_i^{*(1)} + \varepsilon^2\hat{u}_i^{*(2)} + \cdots)$$

$$\hat{p}^* = \varepsilon(\hat{p}^{*(0)} + \varepsilon\hat{p}^{*(1)} + \varepsilon^2\hat{p}^{*(2)} + \cdots)$$

$$\hat{T}^* = \varepsilon(\hat{T}^{*(0)} + \varepsilon\hat{T}^{*(1)} + \varepsilon^2\hat{T}^{*(2)} + \cdots) \tag{23b}$$

Substituting equations (23a) and (23b) into equations (7)–(9), considering the linear perturbation terms only (i.e., ε terms only) and then dropping the unnecessary superscripts, we obtain the following eigenvalue problem:

$$\hat{u}_{i,i}^* = 0 \tag{24}$$

$$\hat{u}_i^* = -\hat{p}_{,i}^* + \mathrm{Ra}\,\hat{T}^* e_i \tag{25}$$

$$\hat{u}_j^* T_{,j}^* + Pe\,\hat{T}_{,2}^* = \hat{T}_{,jj}^* \tag{26}$$

where

$$T_{,1}^* = 0 \quad \text{and} \quad T_{,2}^* = -\mathrm{e}^{Pe\,x_2^*} \tag{27}$$

The corresponding boundary conditions for the perturbation solutions are

$$\hat{T}^* = 0, \qquad \hat{p}^* = p_1^* \qquad (\text{at } x_2^* = 1) \tag{28}$$

$$\hat{u}_2^* = 0, \qquad \hat{T}_{,2}^* = 0 \qquad (\text{at } x_2^* = 0) \tag{29}$$

Note that $\hat{p}^* = 0$ in equation (28) implies that $\partial\hat{u}_2^*/\partial x_2^* = 0$ at $x_2^* = 1$.[10] Inserting

$$\hat{u}_2^* = V(x_2^*)\mathrm{e}^{-\mathrm{i}k_1^* x_1^*}, \qquad \hat{T} = \theta(x_2^*)\mathrm{e}^{-\mathrm{i}k_1^* x_1^*}, \tag{30}$$

into equations (24)–(26) yields

$$V''(x_2^*) - (k_1^*)^2 V(x_2^*) = -(k_1^*)^2\,\mathrm{Ra}\,\theta(x_2^*) \tag{31}$$

$$\theta''(x_2^*) - Pe\theta'(x_2^*) - (k_1^*)^2\theta(x_2^*) = -V(x_2^*)\mathrm{e}^{Pe\,x_2^*} \tag{32}$$

where k_1^* is the dimensionless wave number in the x_1^* direction:

$$k_1^* = k_1 H \tag{33}$$

k_1 being the wave number in the x_1 direction. Using equation (30), equations (28) and (29) can also be rewritten as

$$\theta = 0, \quad V' = 0 \quad (\text{at } x_2^* = 1) \tag{34}$$

$$V = 0, \quad \theta' = 0 \quad (\text{at } x_2^* = 0) \tag{35}$$

Substitution of equation (31) into equation (32) yields the following equation:

$$V^{(\mathrm{IV})}(x_2^*) - PeV'''(x_2^*) - 2(k_1^*)^2 V''(x_2^*) + Pe(k_1^*)^2 V'(x_2^*) + (k_1^*)^2[(k_1^*)^2 - \mathrm{Ra}\,\mathrm{e}^{Pe\,x_2^*}]V(x_2^*) = 0 \tag{36}$$

The analytical solution of equation (36) is troublesome because it contains all order derivatives. Instead we solve equations (31) and (32) approximately through single member Galerkin *ansatze*. The quality of approximation is excellent for Peclet number less than one, as will be shown subsequently by comparison with numerical solutions.

With $V(x_2^*) = A\bar{V}(x_2^*)$ and $\theta(x_2^*) = B\bar{\theta}(x_2^*)$, equations (31) and (32) can be rewritten in the Galerkin form as follows:

$$\int_0^1 [A\bar{V}''(x_2^*) - (k_1^*)^2 A\bar{V}(x_2^*) + (k_1^*)^2 \,\mathrm{Ra}\, B\bar{\theta}(x_2^*)]\,\bar{V}(x_2^*)\,\mathrm{d}x_2^* = 0 \tag{37}$$

$$\int_0^1 [B\bar{\theta}''(x_2^*) - PeB\bar{\theta}'(x_2^*) - (k_1^*)^2 B\bar{\theta}(x_2^*) + \mathrm{A}\bar{V}(x_2^*)\mathrm{e}^{Pe\,x_2^*}]\,\bar{\theta}(x_2^*)\,\mathrm{d}x_2^* = 0 \tag{38}$$

where A and B are independent constants; $\bar{V}(x_2^*)$ and $\bar{\theta}(x_2^*)$ are trial functions for $V(x_2^*)$ and $\theta(x_2^*)$. They must be chosen in such a way that all boundary conditions of the problem are satisfied identically. From equations (37) and (38), it follows that

$$\begin{bmatrix} C_{11} & C_{12} \\ C_{21} & C_{22} \end{bmatrix} \begin{Bmatrix} A \\ B \end{Bmatrix} = \begin{Bmatrix} 0 \\ 0 \end{Bmatrix} \tag{39}$$

where

$$C_{11} = \int_0^1 [\bar{V}''(x_2^*) - (k_1^*)^2\,\bar{V}(x_2^*)]\,\bar{V}(x_2^*)\,\mathrm{d}x_2^*$$

$$C_{12} = \mathrm{Ra}(k_1^*)^2 \int_0^1 \bar{\theta}(x_2^*)\,\bar{V}(x_2^*)\,\mathrm{d}x_2^*$$

$$C_{21} = \int_0^1 \mathrm{e}^{Pex_2^*}\,\bar{V}(x_2^*)\bar{\theta}(x_2^*)\,\mathrm{d}x_2^*$$

$$C_{22} = \int_0^1 [\bar{\theta}''(x_2^*) - Pe\bar{\theta}'(x_2^*) - (k_1^*)^2\,\bar{\theta}(x_2^*)]\,\bar{\theta}(x_2^*)\,\mathrm{d}x_2^* \tag{40}$$

Clearly, the condition, under which equation (39) has a non-zero solution, is

$$C_{11}C_{22} - C_{12}C_{21} = 0 \tag{41}$$

In theory, any function, which satisfies the boundary conditions of the problem considered, can be chosen as the candidate of the trial function. However, in practice, for the purpose of avoiding any unnecessary difficulty in mathematics, it is favourable to use the polynomial function as the trial function because many preliminary functions can be expressed as the combination of polynomial functions using the Taylor expansion. For the hydrothermal system considered, we have tested various candidate trial functions (see Appendix). The best result (minimum error in horizontal wave number at $Pe = 0$) was obtained with

$$\bar{V}(x_2^*) = \tfrac{1}{2}(x_2^*)^2 - x_2^*$$

$$\bar{\theta}(x_2^*) = \tfrac{1}{5}[(x_2^*)^5 - 1] \tag{42}$$

Substituting equation (42) into equation (40) yields the following equations:

$$C_{11} = -\left[\frac{1}{3} + \frac{2}{15}(k_1^*)^2\right]$$

$$C_{12} = \frac{17}{336}\,\mathrm{Ra}(k_1^*)^2$$

$$C_{21} = \frac{1}{Pe^8}\left[e^{Pe}\left(\tfrac{1}{2}Pe^6 - 2Pe^5 + 3Pe^4 + 12Pe^3 - 108Pe^2 + 306Pe - 504\right)\right.$$
$$\left. + \left(504 + 144Pe + \tfrac{1}{5}Pe^5 + \tfrac{1}{5}Pe^6\right)\right]$$

$$C_{22} = -\left[\frac{1}{9} + \frac{1}{33}(k_1^*)^2 - \frac{1}{50}Pe\right] \tag{43}$$

From equations (41) and (43), the critical Rayleigh number, for which temperature driven convective flow may occur, can be expressed as

$$\mathrm{Ra}_{\mathrm{critical}} = \frac{366 C_{11} C_{22}}{17(k_1^*)^2 C_{21}} \tag{44}$$

Since $\mathrm{Ra}_{\mathrm{critical}}$ is a function of $(k_1^*)^2$, its minimum value is obtained from

$$\frac{\partial \mathrm{Ra}_{\mathrm{critical}}}{\partial[(k_1^*)^2]} = 0 \tag{45}$$

Substituting equations (43) and (44) into equation (45) leads to the following condition, under which $\mathrm{Ra}_{\mathrm{critical}}$ has a minimum value for a given Peclet number:

$$k_1^* = \left(\frac{55}{6}\right)^{1/4}\left(1 - \frac{9}{50}Pe\right)^{1/4} \tag{46}$$

Obviously, our approximate solution is only valid for

$$Pe < 50/9 \tag{47}$$

The above restriction is a consequence of the specific trial function we have used in our linear stability analysis and convective solutions may exist (and indeed exist, see Section 3) for $Pe \geqslant 50/9$.

Figure 2 shows the variation of the minimum critical Rayleigh number ($\mathrm{Ra}^*_{\mathrm{critical}}$) with the upward throughflow, which is represented by Pe. In the range considered, $\mathrm{Ra}^*_{\mathrm{critical}}$ decreases as Pe increases, i.e., temperature gradient driven convective flow is destabilized by an increase in upward throughflow. In other words, a decrease in the upward throughflow stabilizes temperature gradient driven convective flow.

3. NUMERICAL ANALYSIS

To confirm our finding that an increase in upward throughflow destabilizes temperature gradient driven convective flow in the hydrothermal system considered, we complement our theoretical

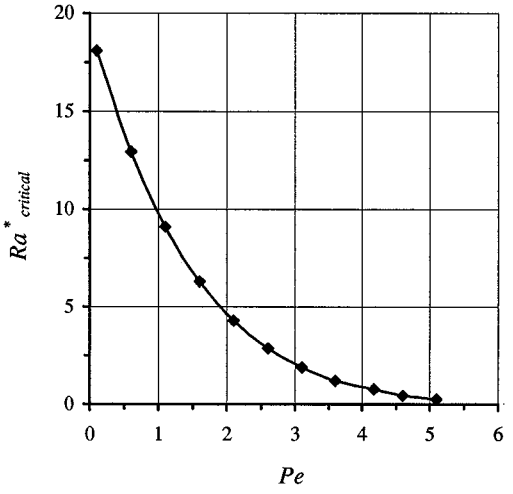

Figure 2. Variation of predicted minimum critical Rayleigh number with the magnitude of throughflow

analysis by a finite element study.[11] Numerical analyses are carried out with the progressive asymptotic approach procedure. The method was thoroughly discussed and validated in a previous study.[2] A brief summary of the finite element formulation is given below.

$$\begin{bmatrix} \mathbf{Q} & -\mathbf{B} \\ \mathbf{0} & \mathbf{E}(\mathbf{U}) \end{bmatrix} \begin{Bmatrix} \mathbf{U} \\ \mathbf{T} \end{Bmatrix} = \begin{Bmatrix} \mathbf{F} \\ \mathbf{G} \end{Bmatrix} \tag{48}$$

where **Q**, **B** and **E** are global property matrices of the system; **U** and **T** are global nodal velocity and temperature vectors of the system; **F** and **G** are global nodal load vectors of the system. They are assembled by the following element property matrices and vectors:

$$\mathbf{Q}^{\mathrm{e}} = \bar{\mathbf{M}}^{\mathrm{e}} + \frac{1}{\varepsilon}\mathbf{A}^{\mathrm{e}}(\mathbf{M}_{\mathrm{p}}^{\mathrm{e}})^{-1}(\mathbf{C}^{\mathrm{e}})^{\mathrm{T}}$$

$$\bar{\mathbf{M}}^{\mathrm{e}} = \begin{bmatrix} \mathbf{M}^{\mathrm{e}} & \mathbf{0} \\ \mathbf{0} & \mathbf{M}^{\mathrm{e}} \end{bmatrix}, \qquad \mathbf{U}^{\mathrm{e}} = \begin{Bmatrix} \mathbf{U}_1^{\mathrm{e}} \\ \mathbf{U}_2^{\mathrm{e}} \end{Bmatrix}, \qquad \mathbf{F}^{\mathrm{e}} = \begin{Bmatrix} \mathbf{F}_1^{\mathrm{e}} \\ \mathbf{F}_2^{\mathrm{e}} \end{Bmatrix}$$

$$\mathbf{B}^{\mathrm{e}} = \begin{Bmatrix} \mathbf{B}_1^{\mathrm{e}} \\ \mathbf{B}_2^{\mathrm{e}} \end{Bmatrix}, \qquad \mathbf{A}^{\mathrm{e}} = \begin{Bmatrix} \mathbf{A}_1^{\mathrm{e}} \\ \mathbf{A}_2^{\mathrm{e}} \end{Bmatrix}, \qquad \mathbf{C}^{\mathrm{e}} = \begin{Bmatrix} \mathbf{C}_1^{\mathrm{e}} \\ \mathbf{C}_2^{\mathrm{e}} \end{Bmatrix}$$

$$\mathbf{M}_{\mathrm{p}}^{\mathrm{e}} = \int_A \boldsymbol{\psi}\boldsymbol{\psi}^{\mathrm{T}}\,\mathrm{d}A, \qquad \mathbf{E}^{\mathrm{e}} = \mathbf{D}_i^{\mathrm{e}}(u_i^*) + \mathbf{L}_i^{\mathrm{e}},$$

$$\mathbf{G}^{\mathrm{e}} = -\int_S \mathbf{q}^*\boldsymbol{\varphi}\,\mathrm{d}S \tag{49}$$

where

$$\mathbf{A}_i^{\mathrm{e}} = \int_A \boldsymbol{\varphi}_{,i}\boldsymbol{\psi}^{\mathrm{T}}\,\mathrm{d}A, \qquad \mathbf{B}_i^{\mathrm{e}} = \int_A \boldsymbol{\varphi}\,\mathrm{Ra}\,\boldsymbol{\varphi}^{\mathrm{T}} e_i\,\mathrm{d}A, \qquad \mathbf{C}_i^{\mathrm{e}} = \int_A \boldsymbol{\psi}\boldsymbol{\varphi}_{,i}^{\mathrm{T}}\,\mathrm{d}A,$$

$$\mathbf{D}_i^{\mathrm{e}}(u_i^*) = \int_A \boldsymbol{\varphi} u_i^* \boldsymbol{\varphi}_{,i}^{\mathrm{T}}\,\mathrm{d}A, \qquad \mathbf{L}_i^{\mathrm{e}} = \int_A \boldsymbol{\varphi}_{,i}\boldsymbol{\varphi}_{,i}^{\mathrm{T}}\,\mathrm{d}A, \qquad M^{\mathrm{e}} = \int_A \boldsymbol{\varphi}\boldsymbol{\varphi}^{\mathrm{T}}\,\mathrm{d}A,$$

$$\mathbf{F}_i^{\mathrm{e}} = \int_S \boldsymbol{\sigma}_i^* \boldsymbol{\varphi}\,\mathrm{d}S, \qquad \boldsymbol{\sigma}_i^* = \frac{K_{\mathrm{h}}\rho_0 c_p}{\mu\lambda_{e0}}\boldsymbol{\sigma}_i, \qquad q^* = \frac{q}{q_0} \tag{50}$$

where $\mathbf{U}_1^{\mathrm{e}}$ and $\mathbf{U}_2^{\mathrm{e}}$ are the dimensionless nodal velocity vectors of the element in the x_1 and x_2 directions, respectively; $\mathbf{A}_i^{\mathrm{e}}$, $\mathbf{B}_i^{\mathrm{e}}$, $\mathbf{C}_i^{\mathrm{e}}$, $\mathbf{E}^{\mathrm{e}}$ and $\mathbf{M}^{\mathrm{e}}$ are the property matrices of the element; $\mathbf{F}_i^{\mathrm{e}}$ and $\mathbf{G}^{\mathrm{e}}$ are the dimensionless nodal load vectors due to the dimensionless stress and heat flux on the boundary of the element; $\boldsymbol{\varphi}$ is the shape function vector for the temperature and velocity components of the element; $\boldsymbol{\psi}$ is the shape function vector for the pressure of the element; $\boldsymbol{\sigma}_i$ and q are the stress and heat flux on the boundary of the element; A and S are the area and boundary length of the element; ε is a penalty parameter since the penalty finite element approach[11] is used to eliminate the pressure variable in the process of deriving equation (48).

From the finite element computational point of view, the problem domain must be finite in size. This is in contradiction with the hydrothermal system considered here because it is a horizontal layer of infinite length. However, consideration of the periodic nature of the solutions (see equation (30)) for high Rayleigh numbers makes it possible to overcome this difficulty. Theoretically, it is appropriate to place two vertical boundaries of the finite element computational domain at the cell boundaries, where both the horizontal velocity and the normal thermal flux are zero. Since there are two cells (a clockwise cell and an anticlockwise cell) in a periodic cycle of the solutions, the length of a cell in the horizontal direction is equal to half the wavelength of the system. This indicates that the minimum length of the finite element computational domain should equal half the wavelength of the system. From equation (33), such a minimum length can be deduced and expressed as

$$L^* = L/H = \pi/k_1^* \tag{51}$$

where L is half the wavelength of the system; L^* is the minimum dimensionless length of the finite element computation domain and can be estimated using equations (51) and (46). Figure 3 shows the computation domain, which is discretized into 2304 four-node quadrilateral element with 2401 nodes in total.

Figure 4 shows the comparison of the analytical results with the numerical results. It needs to be pointed out that the analytical results are calculated using equations (43), (44) and (46), which are based on linear stability theory and the Galerkin method. The numerical results are obtained in the following manner. For a given Peclet number, L^* is estimated using equations (46) and (51) and a finite element model is established. Note that $Pe = 6$, L^* is negative. In this case, L^* is estimated using $Pe = 5$, instead of $Pe = 6$. By varying the Rayleigh numbers, the same model is repeatedly used to calculate the convection cell until the minimum Rayleigh number, below

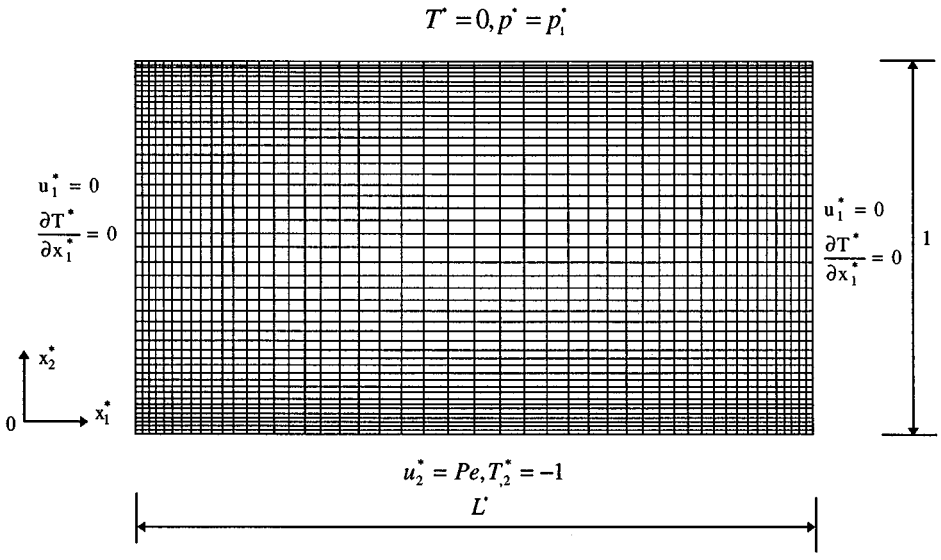

Figure 3. Finite element mesh for the hydrothermal system

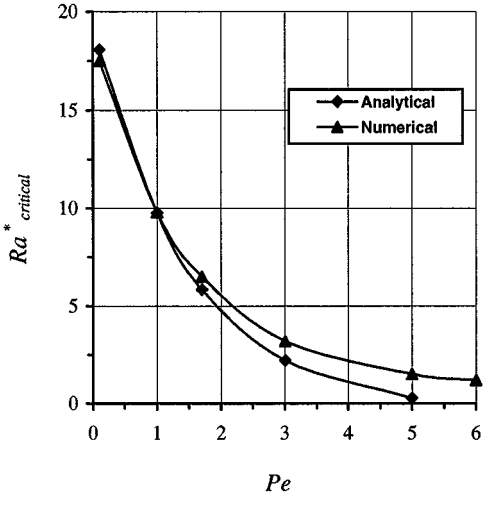

Figure 4. Comparison of analytically predicted results with numerically calculated results

which temperature gradient driven flow does not take place, is determined. It is obvious from Figure 4 that the numerical results agree well with the analytical ones. Both the numerical and analytical results demonstrate that the minimum critical Rayleigh number decreases as the Peclet number increases.

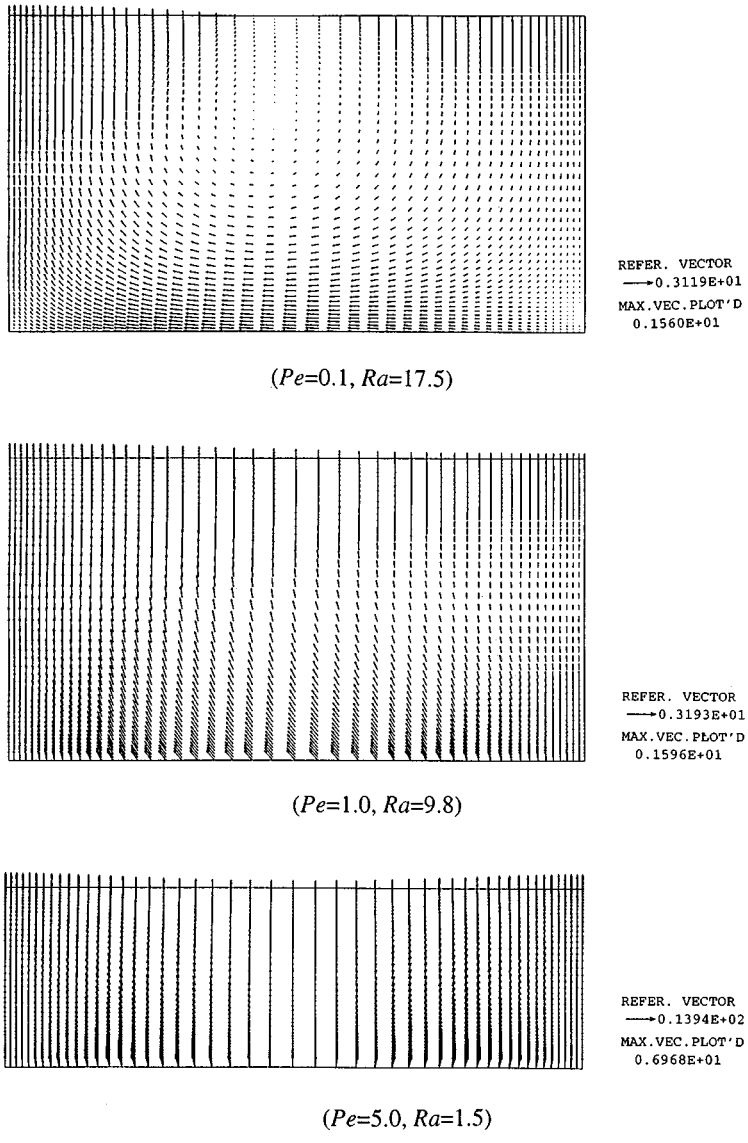

Figure 5. Dimensionless total velocity distribution due to different upward throughflow

Figures 5 and 6 show the dimensionless total velocity and perturbation velocity distribution due to different upward throughflow conditions. The perturbation velocity is calculated by taking the trivial velocity from the total velocity. Figure 5 shows that the Peclet number Pe has a significant effect on the pattern of total convective flow in the hydrothermal system. Since the perturbation velocity is induced by the temperature gradient only, the corresponding convection cells are clearly exhibited in Figure 6.

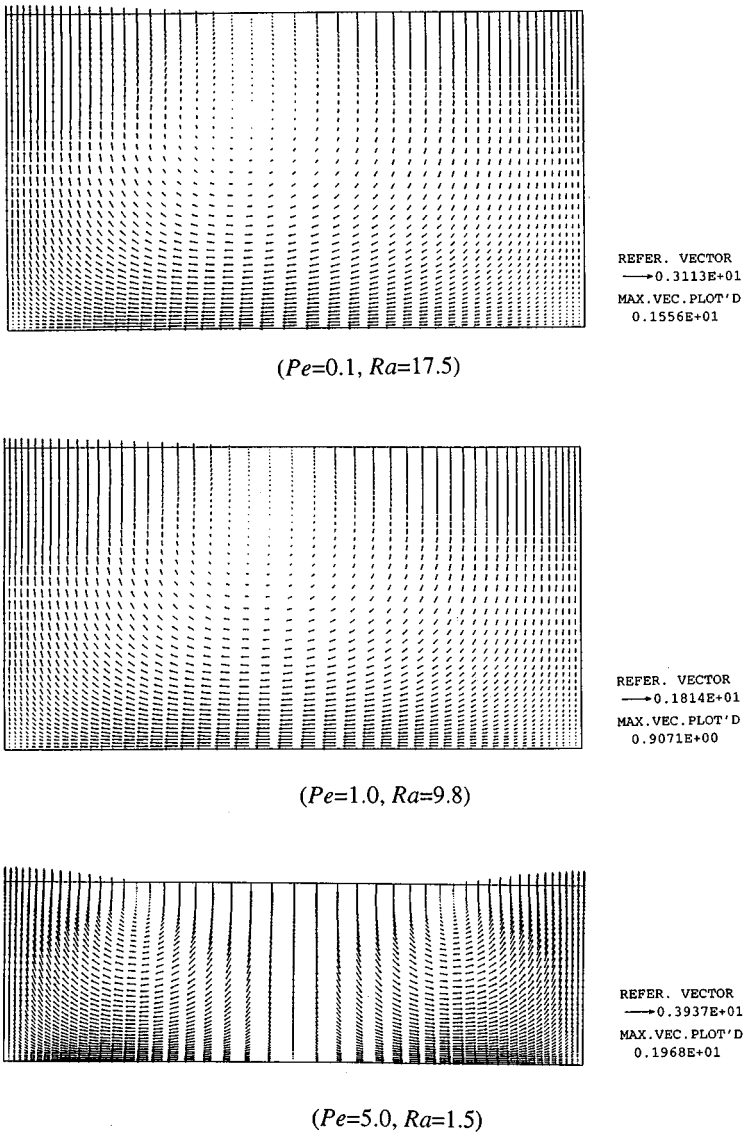

Figure 6. Dimensionless perturbation velocity distribution due to different upward throughflow

Figure 7 shows the dimensionless temperature distribution in the hydrothermal system due to non-uniform upward throughflow. If temperature gradient driven convective flow does not occur, the isotherms are horizontal lines. However, once temperature gradient driven convective flow takes place, the isotherms become curved lines. Since the distance between two neighbouring isotherms represents the magnitude of the temperature gradient, Figure 7 shows that the

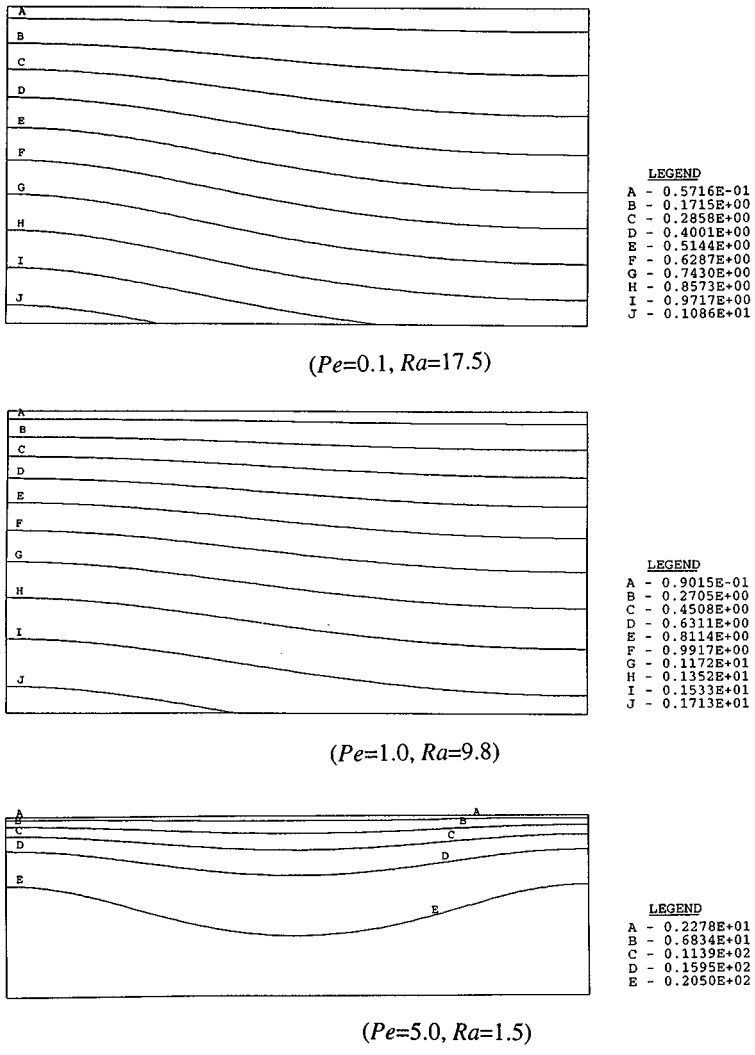

Figure 7. Dimensionless temperature distribution due to different upward throughflow

temperature gradient at the top of the layer becomes much larger than that at the bottom of the layer. Generally, the temperature gradient at the top of the layer increases as the Peclet number *Pe* increases, as is indicated by equation (18).

To investigate the effect of temperature gradient driven convective flow on ore body formation and mineralization in permeable rock masses, the dimensionless Rock Alternation Index (RAI)[8] has been calculated and shown in Figure 8 for three different upward throughflow cases. According to Phillips,[8] the RAI is defined as the dot product of the pore-fluid velocity

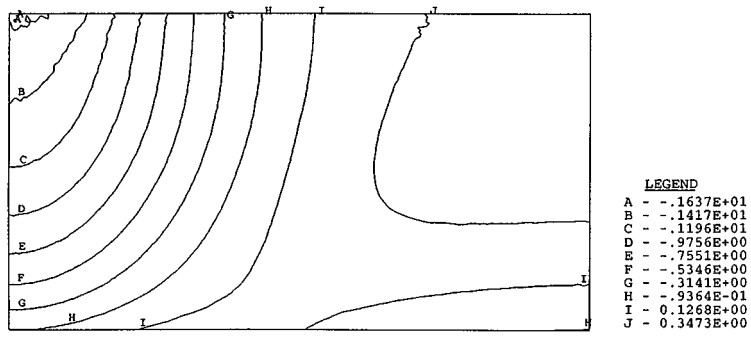

(*Pe*=0.1, *Ra*=17.5)

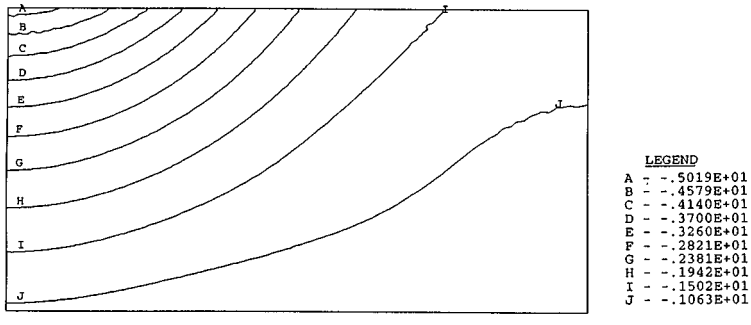

(*Pe*=1.0, *Ra*=9.8)

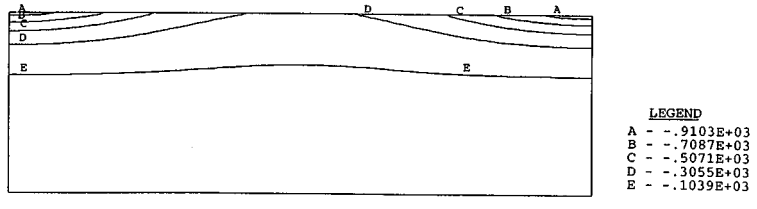

(*Pe*=5.0, *Ra*=1.5)

Figure 8. Dimensionless *RAI* distribution due to different upward throughflow

and temperature gradient. Physically, the down temperature pore-fluid flow most likely results in minerals precipitation, whereas the up temperature pore-fluid flow most likely results in minerals dissolution in a hydrothermal system. This implies that for temperature gradient driven mineralization, the minimum negative value of the rock alteration index indicates the most probable region of mineral precipitation. Without temperature gradient driven convective flow, the isopleth of the rock alteration index is horizontal.

Figure 8 shows that the most probable region of mineral precipitation is remarkably localized and concentrated.

4. CONCLUSIONS

For the hydrothermal system considered in this paper, the exact analytical solutions indicate that the trivial horizontal and vertical Darcy velocities are zero (equation (13)) and constant (equation 15)), respectively, throughout the whole layer. The trivial temperature profile is of a non-linear nature along the layer thickness direction and is given by equation (18).

From linear stability theory and the Galerkin method, it has been demonstrated that the hydrothermal system becomes unstable when the Rayleigh number is equal to or greater than the minimum critical Rayleigh number of the system. To represent the hydrothermal system considered here, the modified Rayleigh number used is expressed as a function of the injected conductive thermal flux at the bottom of the layer. In addition, it has also been demonstrated that the minimum critical Rayleigh number only depends on the upward throughflow (Pe) within the range considered in this study. This implies that the onset of temperature gradient driven convective flow in the hydrothermal system considered is only dependent on the bottom temperature gradient, upward throughflow and the hydrothermal parameters of the system, but independent of the initial pressure distribution within the layer. The reason for this is due to the fact that the convective flow is driven by the temperature gradient, rather than by the initial pressure gradient in the hydrothermal system.

Both theoretical and numerical analyses have indicated that for a small or moderate Pe (up to $Pe \leqslant 6$), an increase in upward throughflow destabilizes the temperature gradient driven flow in the hydrothermal system considered. This implies that within the range of $Pe \leqslant 6$, the occurrence of temperature gradient driven convective flow becomes easier as the upward throughflow becomes stronger, for a layer of given thickness.

It is concluded from the related numerical results that not only can temperature gradient driven convective flow occur in systems with upward throughflow, but also it potentially plays an important role in the process of ore body formation and mineralization in the hydrothermal system considered.

ACKNOWLEDGEMENTS

The authors are very grateful to the anonymous referees for the valuable comments on an early draft of this paper.

APPENDIX

In the case of $Pe = 0$, the analytical solution to the dimensionless horizontal wave number in correspondence with the minimum critical Rayleigh number for the hydrothermal system considered[10] is equal to 1·75. Thus, error in the dimensionless horizontal wave number resulted from different groups of trial functions can be compared with this analytical solution, as shown in Table I below.

Table I. Comparisons of different trial functions ($Pe = 0$)

Group	Trial functions	Dimensionless horizontal wave number	Relative error (%)
1	$\bar{V}(x_2^*) = \frac{1}{2}(x_2^*) - x_2^*, \quad \bar{\theta}(x_2^*) = \frac{1}{2}[(x_2^*)^2 - 1]$	$k_1^* = \sqrt[2]{\left(\frac{5}{2}\right)}$	9·71
2	$\bar{V}(x_2^*) = \frac{2}{3}(x_2^*)^{3/2} - x_2^*, \quad \bar{\theta}(x_2^*) = \frac{2}{3}[(x_2^*)^{3/2} - 1]$	$k_1^* = \sqrt[4]{\left(\frac{105}{16}\right)}$	8·57
3	$\bar{V}(x_2^*) = \frac{1}{2}(x_2^*)^2 - x_2^*, \quad \bar{\theta}(x_2^*) = \frac{2}{3}[(x_2^*)^{3/2} - 1]$	$k_1^* = \sqrt[4]{\left(\frac{75}{12}\right)}$	9·71
4	$\bar{V}(x_2^*) = \frac{2}{3}(x_2^*)^{3/2} - x_2^*, \quad \bar{\theta}(x_2^*) = \frac{1}{2}[(x_2^*)^2 - 1]$	$k_1^* = \sqrt[4]{\left(\frac{105}{16}\right)}$	8·57
5	$\bar{V}(x_2^*) = \frac{2}{3}(x_2^*)^{3/2} - x_2^*, \quad \bar{\theta}(x_2^*) = \frac{4}{5}[(x_2^*)^{5/4} - 1]$	$k_1^* = \sqrt[2]{\left(\frac{63}{24}\right)}$	7·43
6	$\bar{V}(x_2^*) = \frac{1}{3}(x_2^*)^3 - x_2^*, \quad \bar{\theta}(x_2^*) = \frac{1}{2}[(x_2^*)^2 - 1]$	$k_1^* = \sqrt[4]{\left(\frac{2625}{482}\right)}$	12·6
7	$\bar{V}(x_2^*) = \frac{1}{2}(x_2^*)^2 - x_2^*, \quad \bar{\theta}(x_2^*) = \frac{1}{3}[(x_2^*)^3 - 1]$	$k_1^* = \sqrt[4]{7}$	6·86
8	$\bar{V}(x_2^*) = \frac{1}{2}(x_2^*)^2 - x_2^*, \quad \bar{\theta}(x_2^*) = \frac{1}{4}[(x_2^*)^4 - 1]$	$k_1^* = \sqrt[4]{\left(\frac{225}{28}\right)}$	4·00
9	$\bar{V}(x_2^*) = \frac{1}{2}(x_2^*)^2 - x_2^*, \quad \bar{\theta}(x_2^*) = \frac{1}{5}[(x_2^*)^5 - 1]$	$k_1^* = \sqrt[4]{\left(\frac{55}{6}\right)}$	0·57

REFERENCES

1. C. Zhao and G. P. Steven, Analytical solutions for tansient diffusion problems in infinite media', *Comput. Methods Appl. Mech. Engng*, **129,** 29–42 (1996).
2. C. Zhao, H. B. Mühlhaus and B. E. Hobbs, 'Finite element analysis of steady-state natural convection problems in fluid-saturated porous media heated from below', *Int. J. Numer. Anal. Methods Geomech.*, **21,** 863–881 (1997).
3. C. Zhao, H. B. Mühlhaus and B. E. Hobbs, 'Effects of geological inhomogeneity on high Rayleigh number steady-state heat and mass transfer in fluid-saturated porous media heated from below', *Int. J. Comput. Method. Numer. Heat Transfer*, **33,** 415–431 (1998).
4. C. Zhao, B. E. Hobbs and H. B. Mü hlhaus, 'Finite element modelling of temperature gradient driven rock alteration and mineralization in porous rock masses', *Comput. Methods Appl. Mech. Engng.*, **165,** 175–187 (1998).
5. M. C. Jones and J. M. Persichetti, 'Convective instability in packed beds with throughflow', *A.I.Ch.E. J.*, **32,** 1555–1557 (1986).
6. D. A. Nield, 'Convective instability in porous media with throughflow', *A.I.Ch.E. J.*, **33,** 1222–1224 (1987).
7. D. N. Riahi, 'Non-linear convection in a porous layer with permeable boundaries', *Int. J. Non-Linear Mech.*, **24,** 459–463 (1989).
8. O. M. Phillips, *Flow and Reactions in Permeable Rocks*, Cambridge University Press, Cambridge, 1991.
9. D. A. Nield and A. Bejan, *Convection in Porous Media*, Springer, New York, 1992.
10. D. A. Nield, 'Onset of thermohaline convection in a porous medium', *Water Resour. Res.*, **4,** 553–560 (1968).
11. O. C. Zienkiewicz, *The Finite Element Method*, McGraw-Hill, London, 1977.

